

Weighing the cusp at the Galactic Centre

N. Mouawad¹, A. Eckart¹, S. Pfalzner¹, R. Schödel¹, J. Moustaka¹, and R. Spurzem²

¹ I. Physikalisches Institut, Universität zu Köln, Zülpicher Str. 77, 50937 Köln, Germany

² Astronomisches Recheninstitut, Mönchhofstr. 12-14, 69120 Heidelberg, Germany

Received ; accepted ,

Abstract. As stars close to the galactic centre have short orbital periods it has been possible to trace large fractions of their orbits in recent years. Previously the data of the orbit of the star S2 have been fitted with Keplerian orbits corresponding to a $3\text{-}4 \times 10^6 M_\odot$ massive black hole (MBH). However, it has also been shown that the central black hole resides in a $\sim 1''$ diameter stellar cluster of a priori unknown mass. In a spherical potential which is neither Keplerian nor harmonic, orbits will precess resulting in rosetta shaped trajectories on the sky. In this case, the assumption of non-Keplerian orbits is a more physical approach. It is also the only approach through which cusp mass information can be obtained via stellar dynamics of the cusp members. This paper presents the first exemplary modelling efforts in this direction. In addition to the solution of a $3.7 \times 10^6 M_\odot$ black hole with insignificant cusp mass, we obtain best fits for a total (MBH plus cusp) mass of $4.1 \times 10^6 M_\odot$ with 10% extended component and $4.8 \times 10^6 M_\odot$ total mass with a 25% extended component. While high total masses above $\sim 5 \times 10^6 M_\odot$ are in conflict with enclosed mass estimates at larger radii, there is no contradiction for the 10% cusp mass solution which is discussed in detail. It is unlikely that such a high extended mass is composed of sub-solar mass constituents, but could be explained rather well by a cluster of high M/L stellar remnants, which we find to form a stable configuration.

Key words. Galactic Centre – Stellar dynamics – Stellar cluster – Cusp – Black Hole

1. Introduction

Over the last decade, evidence has been found for the existence of massive black holes (MBH) in the centres of many nearby galaxies. With increasing observational data – 12 MBHs candidates detected until 1995 (Kormendy & Richstone 1995), and more than 37 until 2001 (Kormendy 2001, Ferrarese et al. 2001) – it is argued that most galaxies harbour nuclei dominated by MBHs with masses that range between 10^6 and $10^{9.5}$ solar masses.

Located at a distance of only ~ 8 kpc from the solar system (Reid 1993; Eisenhauer 2003), the Galactic Centre (GC) is the closest and therefore best object for investigating physical processes in the galactic nucleus of a typical spiral galaxy. It offers a unique “laboratory” for studying stars and gas in the sphere of influence of a super-massive black hole, (e.g., Genzel, Hollenbach, & Townes 1994; Morris & Serabyn 1996; Mezger, Duschl, & Zylka 1996; Melia & Falcke 2001), with a degree of detail that cannot be accessed in any other galactic nucleus in the foreseeable future. With the now available high sensitivity and angular resolution, large ground-based telescopes offer the opportunity to obtain an unprecedented view of the Galactic centre. Initially, with speckle imaging techniques and lately with adaptive optics techniques, high angular resolution images on the Galaxy’s central cluster were obtained. This first set of observations was able to measure stellar motions on the plane of the sky, yielding estimates of the projected veloci-

ties (Eckart & Genzel 1996; Ghez et al. 1998), projected accelerations (Ghez et al. 2000; Eckart et al. 2002a), and three-dimensional orbital motions (Schödel et al. 2002, 2003; Ghez et al. 2003b), which each provided a successively stronger case for a super-massive black hole at the centre of the Milky Way and its association with the unusual radio source Sgr A* (Lo et al. 1985).

More than a decade of high-resolution infrared observations of proper motions in the GC, with the ESO New Technology Telescope (NTT) and the ESO Very Large Telescope (VLT) (Eckart & Genzel 1996; Eckart et al. 2002a; Schödel et al. 2002, 2003), as well as with the Keck telescope (Ghez et al. 1998, 2000, 2003b), have revealed at least 6 stars that show substantial acceleration due to the super-massive black hole associated with Sgr A* and are on bound orbits around it. With a peri-centre of less than 0.6 mpc (15 mas) and an orbital period of ~ 15 years, S2 is the most striking case of these.

A series of observations with the NAOS/CONICA adaptive optics system/near-infrared camera at the ESO VLT unit telescope 4 that covered the peri-centre passage of the star S2 around Sgr A* allowed Schödel et al. (2002) to approximate a Keplerian orbit and to measure the enclosed dark mass down to a distance of ~ 0.6 mpc from Sgr A*. With these observations, they could exclude a neutrino ball scenario (Munyaneza & Viollier, 2002) as an alternative explanation for the dark mass concentration. They excluded as well a cluster of dark

astrophysical objects (Maoz 1998) such as neutron stars, leaving a central super-massive black hole as the most probable explanation.

Using the Keck 10m telescope, Ghez et al. (2003a) confirmed and improved Schödel et al. (2002) results and reported the first spectroscopic identification and line-of-sight velocity measurement of S2. The first detection of spectral absorption lines by Ghez et al. (2003a) (both Bry ($2.1661\ \mu\text{m}$) and He I ($2.1126\ \mu\text{m}$)), provided line-of-sight velocity measurements. These measurements resolved the ambiguity on the inclination of the S2 orbit indicating that its position was behind the black hole when it passed through its peri-centre. In addition, stellar rotational velocities suggest that S2 is an O8-B0 dwarf star and thus a massive ($\sim 15\ M_{\odot}$) young star ($\leq 10\ \text{Myrs}$).

From data taken with NAOS/CONICA and the new NIR integral field spectrometer SPIFFI at the ESO VLT, Eisenhauer et al. (2003) reported new astrometric observations and additional spectroscopic observations of the star S2, reducing the uncertainties on the orbital parameters. They also gave the most accurate primary distance measurement to the centre of the Milky Way of $7.94 \pm 0.42\ \text{kpc}$, which is in agreement with earlier determinations (see Reid 1993).

In this paper, we explore the possibility that there exists a compact, continuous mass distribution composed of several undetectable faint stars or perhaps some more exotic material in addition to the point mass of Sgr A*. In this case, the orbit of S2 will not follow a simple Keplerian orbit, but will rather show peri-centre-shifts that result in rosetta shaped orbits. This idea is motivated by the observation that the stellar density does not flatten out, but exhibits a steep peak towards the centre, a so-called cusp (Eckart et. al, 1995; Alexander et. al, 1999; Genzel et al, 2003). In contrast to earlier studies, the main approach of this work is that the mass-to-light ratio, M/L , is *not* considered to be constant over the entire range of the GC stellar cluster. There are indications that the stellar population varies with position and is not quite well mixed (Alexander 1999). The exact composition of the cusp is still unknown and our current understanding of the stellar distribution in the GC is incomplete (Genzel et al. 2003). With current observations, low-mass stars ($K \leq 21\ \text{mag}$) cannot be observed in these dense cusp regions and the true value of the M/L ratio is not known. The approximation that the dynamics in the central region is Keplerian is directly related to the implicit assumption that the M/L ratio at $2\ \mu\text{m}$ in the cusp is as low as in the outer stellar cluster ($M/L = 2M_{\odot}/L_{\odot}$). As pointed out by Baumgardt et al. (2003), dynamical evolution of a dense stellar cluster will inevitably lead to a strongly increasing M/L ratio by segregation of stellar evolution remnants to the centre.

Considering these circumstances, stars with short orbital periods, in particular the star S2, of which orbital data are best known, play a key role in exploring the gravitational potential. We show that the present observational data on S2 cannot discriminate between a *Keplerian* and a *non-Keplerian* potential. Subsequently, we study the influence of an extended distribution of dark mass near Sgr A* taking into consideration the constraints set by the orbit of S2. In this study relativistic effects are neglected as they are second order corrections.

In § 2 we outline our modelling of the density distribution of the central region and show that the star counts near Sgr A* can be described by a compact Plummer model core. The method used to compute orbits in non-Keplerian potentials is explained in § 3. In § 4 possible orbital models for S2 are presented. We discuss the implications of *Keplerian* and *non-Keplerian* orbits for the mass distribution near Sgr A* in § 5, and draw our conclusions in § 6.

2. Modelling the stellar cluster and the enclosed mass

In this section it is described how the most recent observations of the GC star cluster (Genzel et al., 2000, 2003) can be used to model the mass distribution function as close as a few milli-parsec from Sgr A*. A surface density profile is fitted to number density counts and used, together with dynamical mass estimators, to deduce the 3 dimensional mass distribution function.

2.1. Density model of the stellar cluster

Genzel et al. (2003, see their Fig.7) determined the surface number density of stars in the central parsec by counting the sources in annuli with increasing radius around Sgr A*. Within $\sim 2\ \text{arc-seconds}$ of Sgr A*, their data indicate an excess of faint stars above the counts expected in a cluster with a flat core, as it had been already suggested earlier (Eckart et al. 1995; Alexander 1999). They confirmed the existence of a "cusp" and showed that it is centred at a position of $(\Delta\alpha, \Delta\delta) = (+0.09^\circ, -0.15^\circ)$ from Sgr A*, with an uncertainty of $\pm 0.2^\circ$. Here we use the same K-band counts ($K \leq 18$) together with the earlier SHARP/NTT counts ($K \leq 15$), without taking into our study their higher magnitude limit H-band counts ($H \leq 19$). In contrast to the 'by-eye' H-band counts, the K-band counts, were determined by an automated procedure, they are therefore possibly less biased, and cover the whole range of the cluster, not only the central arc-second.

Genzel et al. (2003) fitted a broken power-law to their stellar counts, with a distinct break at $10\ \text{arcsec}$. In this section, we show that it is also possible to fit the number density counts with a superposition of several Plummer models. The Plummer model has the advantage of being analytically integrable. It resembles actual clusters with compact cores and an extended outer envelope (Spitzer 1975). In this model the 3 dimensional radial density distribution $\rho(r)$ and the projected mass density $\sigma(r)$ are described by:

$$\rho(r) = \frac{3M}{4\pi R^3} \frac{1}{(1 + \frac{r^2}{R^2})^{\frac{5}{2}}}, \quad (1)$$

$$\sigma(r) = \frac{4\rho(0)R}{3} \frac{1}{(1 + \frac{r^2}{R^2})^2}, \quad (2)$$

where R is the core radius and M the total mass.

Our best surface density fit to the data consists of a superposition of 6 different Plummer models, which will be termed in the following as 'composite model':

$$\sigma(r) = \sum_{i=1}^6 \frac{M_i}{\pi} \frac{R_i^2}{(r^2 + R_i^2)^2}. \quad (3)$$

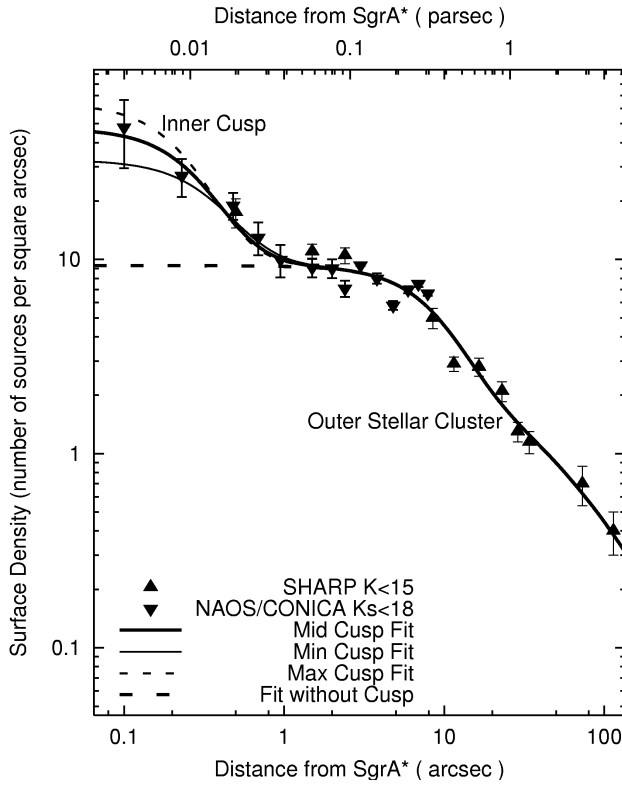


Fig. 1. Surface density of stars vs. distance from Sgr A*. The downward pointing triangles represent the CONICA/NAOS data for $K_s \leq 18$, the upward pointing triangles are SHARP/NTT data for $K_s \leq 15$ stars scaled up by a factor of 5 in order to match the fainter NAOS/CONICA counts. The data are taken from Genzel et al. (2000, 2003). The long-dashed line is the superposition of the 5 outermost Plummer models (see, Table 1). The addition of the innermost Plummer model (the 'inner' cusp) gives the 'composite model'. It is represented by the 3 other curves, where the thick-straight line corresponds to the middle values of the 'inner cusp' parameters R_1 and M_1 , the thin-straight line to its lower values, and the short-dashed line to its upper values.

The six values of the core radii, R_i , are given in Table 1. Fig. 1 shows that there exists a mini-core centred on Sgr A*, which we denominate as the 'inner cusp'. It is represented by the innermost Plummer model with a core radius $R_1 = 15.5\text{ mpc} \cong 0.4''$. The combination of the five outermost components gives a similar configuration as the flattened isothermal sphere of core radius $\sim 0.3\text{ pc}$ derived by Genzel et al. (2003).

With an apo-centre of approximately 9 mpc (Schödel, 2004; Ghez et al., 2003a), the star S2 orbits in a region inside the core radius ($R_1 \sim 15\text{ mpc}$) of this innermost model. Therefore its path can be mainly influenced, in addition to the BH potential, by the 'inner cusp' gravitational potential. At these distances from the centre, the present number density counts have large error bars (see Fig. 1). The limits on the core radius, R_1 , of our model, deduced from the error bars on the number density counts, are found to be 13.8 mpc for the lower value R_1^{\min} , and 20.2 mpc for the upper one R_1^{\max} . Varying the mass, M_1 , of the central Plummer model component allows to study cases

Table 1. The parameters of the 'composite model' used to fit the GC stellar cluster. For each Plummer model we give the value of the core radius R_i (in arcsec and in parsec) deduced from the surface density plot. M_i is the corresponding total mass scaled to the enclosed mass distribution (Fig. 2). ρ_i is the calculated average density. The first Plummer model ($R_1 = 0.4''$ or 0.015 mpc) corresponds to the inner cusp centred at Sgr A*. The addition of the remaining 5 models represents the density distribution of the outer stellar cluster.

i	$R_i[\text{arcsec}]$	$R_i[\text{pc}]$	$M_i[\text{M}_\odot]$	$\rho_i(0)[\text{M}_\odot \cdot \text{pc}^{-3}]$
1	0.4	0.015	8540	6.0×10^8
2	13	0.5	1.8×10^6	3.5×10^6
3	52	2.0	2.7×10^6	7.9×10^4
4	97	3.8	6.7×10^6	2.9×10^4
5	220	8.5	13.1×10^6	5.1×10^3
6	321	12.4	27.6×10^6	3.4×10^3

in which the mass-to-light ratio, M/L , varies as a function of distance from Sgr A*. As described in § 3 and § 4, exploring the possible ranges for R_1 and M_1 that fulfill the constraints given by the orbital measurements of star S2 allows us to derive dynamical information on the cusp mass.

The density of the 'inner cusp' is a few hundred times larger than that of the next outer stellar cluster and it has a ~ 33 times smaller core radius (see Fig. 1 and Table 1). Our model implies density values as high as $1.68 \times 10^8 \text{ M}_\odot \text{pc}^{-3}$ at $0.1''$, and $1.54 \times 10^7 \text{ M}_\odot \text{pc}^{-3}$ at $1''$. These values are comparable to the ones derived by Genzel et al. (2003) from a broken power-law density profile ($7 \times 10^8 \text{ M}_\odot \text{pc}^{-3}$ at $0.1''$ and $3 \times 10^7 \text{ M}_\odot \text{pc}^{-3}$ at $1''$).

2.2. The enclosed mass

Similarly to eq.3, the mass distribution of the 'composite model' is given by

$$M(r) = \sum_{i=1}^6 \frac{M_i r^3}{(r^2 + R_i^2)^{3/2}}. \quad (4)$$

This equation can be scaled and fitted to the dynamical mass estimates vs. distance as they were determined by Genzel et al. (2000), Ott (2003), and Eisenhauer et al. (2003) (see Fig. 2). Our best fit corresponds to a $2.9 \times 10^6 \text{ M}_\odot \pm 0.3 \times 10^6 \text{ M}_\odot$ black hole plus the mass distribution of eq.4, of which the 6 total masses M_i , are listed together with their corresponding densities, ρ_i , in Table 1. Our compact mass value is in good agreement with the value of $3.6 \pm 0.6 \times 10^6 \text{ M}_\odot$ based on the orbit of S2 as recently derived by Eisenhauer et al. (2003) and (again based on S2) confirmed in § 4. An offset in the value of the enclosed compact mass will not influence our modelling significantly because the shape and mass of our cluster composite model depends primarily on the profile of the stellar number counts.

In Fig. 2 the long-dashed line corresponds to our best fit, the thick-straight line shows only the enclosed mass without a BH obtained with our model of the extended cluster. The

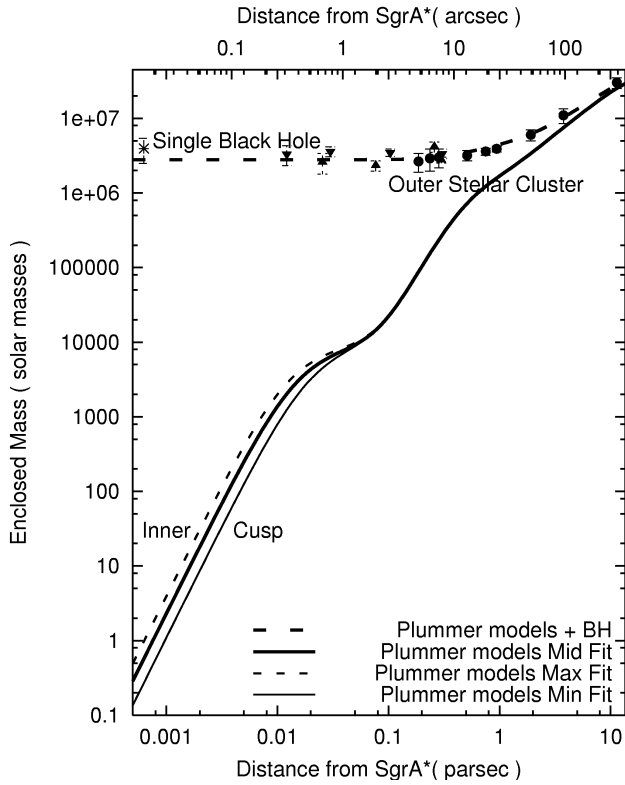


Fig. 2. Mass distribution in the central 10 pc of the Galactic Centre for an 8 kpc distance (Reid et al. 2003; Eisenhauer et al., 2003). Filled circles are mass estimates from a parameterised Jeans-equation model of the radial velocities of late type stars, assuming isotropy (Genzel et al. 2000). Filled downward-pointing triangles denote Leonard-Merritt projected mass estimators from a new NTT proper motion data set (Ott 2003). The star point denotes the mass derived from the orbit of S2. The error bar combines the orbital fit and astrometry errors (Eisenhauer et al. 2003). The long-dashed line is a fit to the measured enclosed mass against distance. That results from a combination of the mass distributions (see § 2.2) deduced from the composite model fit to the stellar cluster, plus a $2.9 \times 10^6 M_\odot$ black hole. The same model without a point mass is represented by the 3 other curves, they correspond to acceptable models within the error bars.

thin-straight and the short-dashed lines represent the above discussed extreme cases of an inner cusp radius $R_1 = R_1^{\min} = 13.8$ mpc with $M = 8540_\odot$ and $R_1 = R_1^{\max} = 20.2$ mpc with $M = 8820_\odot$. Note that these errors result from the uncertainties of the stellar number counts at the smallest distances to Sgr A* (Fig. 1).

In the following we will use the above derived mass distribution to determine the path of S2 in response to this non-point mass potential.

3. Modelling the Orbit of S2

In order to fit non-Keplerian orbits to the measured time-dependent positions of the star S2 in the above described type of mass potential, one needs a high accuracy integrator. For this purpose, we chose a fourth order Hermite integrator

Table 2. Characteristic χ^2_{tot} of our fits. The right column lists the corresponding number of data points for which the resulting orbit lies within their 1σ error bars.

χ^2_{tot}	quality of fit
[1.05 : 1.2]	95%-90% of data points \in curve
[1.2 : 1.5]	90%-80% of data points \in curve
[1.5 : 1.7]	80%-75% of data points \in curve
[1.7 : 1.9]	75%-70% of data points \in curve
[1.9 : 2.0]	70%-65% of data points \in curve
> 2.0	3σ level error for at least one point

derived from the one used in high-accuracy N -body simulations (Aarseth 1999, Spurzem 1999, for an introduction of the Hermite scheme see Makino & Aarseth 1992). The advantage of the Hermite scheme is that it allows a fourth order accurate integration based on only two time steps. Therefore it requires the analytic computation of the time derivative of the gravitational force. This is the point where the integrability of the Plummer model is convenient. We computed the trajectory of S2 around the BH and through the extended mass as given by our mass model (see § 2). The presence of an extended mass induces retrograde pericenter-shifts which result in open rosetta shaped orbits.

In total there are nine fit parameters - six orbital elements, the total central mass M_{tot} , the fraction f of the extended mass to the total mass M_{tot} , and the position P of the central mass. All these values are known within a certain margin. We used the position measurements for S2, the dynamical position of Sgr A* and the 5 line-of-sight velocity measurements as determined by Schödel et al. (2003) and Eisenhauer et al. (2003).

A valid computed orbit has to fit both the measured velocities and positions. Therefore, two χ^2 values, one for the positions, χ^2_{pos} , and another for the velocities, χ^2_{vel} , were estimated. We considered the χ^2 values for the positions and velocities independently because the χ^2 values for the velocities were, in general, relatively much smaller than for the positions. In some cases they indicated that measurement errors were systematically overestimated. Therefore χ^2_{vel} were scaled to χ^2_{pos} , and taking into account that we have about 10 times more positional (in R.A. and Dec.) than radial velocity measurements, both values were weighted in order to define a common reduced χ^2 , χ^2_{tot} according to:

$$\chi^2_{tot} = \frac{9}{10}(\chi^2_{pos} + \frac{\chi^2_{vel}}{9}). \quad (5)$$

Table 2 lists the obtained characteristic χ^2_{tot} values together with corresponding percentages of measured data lying on the resulting orbit within their 1σ error bars.

3.1. Influence of model parameters

When modelling the orbits the initial parameters have to be varied over a large parameter space. This large space cannot be fully covered with a reasonable computational effort. In order to study the main effects of a varying cusp mass on the orbit of

star S2 we decided to investigate a representative coverage of the parameter space that still includes the full range of possible scenarios. In total 180 orbits were computed and fitted to the data.

3.1.1. Orbital Elements as Initial Parameters

The six independent elements correspond to the three velocities and three coordinates, that determine the orbit dynamically. From the imaging data, sky positions and proper motions are given in a certain error range for each epoch. For a chosen initial epoch, six input values are varied within certain limits. This leads to a number of N^6 orbital runs for each fitting procedure (N = number of steps per parameter). At the end of each run a χ^2 value was estimated (see section 3.1), constructing this way a 6D-grid of χ^2 values. In order to reduce computation time, in a second step, only for the cases with relatively low χ^2 the orbits were recalculated with a higher temporal resolution, i.e. smaller time step. We recomputed each of these cases separately looking at higher resolution, but in a smaller parameter range, for the best fitting orbit. This iteration was repeated a few times till the necessary precision was reached.

3.1.2. Central Mass as Initial Parameter

The orbit of S2 is studied assuming two components - the mass of the black hole and an extended component. The black hole is treated as a point mass. From previous works it is known that a BH of $\sim 3 \times 10^6 M_\odot$ is present at the centre of our Galaxy. This mass is associated with the compact radio source Sgr A* (Schödel et al. 2003, Ghez et al. 2003). From limits of its proper motion Reid et al. (2003) deduced a lower limit of this mass at $5 \times 10^5 M_\odot$. It has also been shown that the mass is unlikely to exceed $4.8 \times 10^6 M_\odot$ (Ghez et al. 2003; Schödel et al. 2003). In our simulations, the value of the central mass is varied in this mass range, considering six values of M_\odot – estimates of the best fitting values from different observational works (Genzel et al. 2000, Schödel et al. 2003, Ghez et al. 2003). In addition, for any of these given total central mass values, M_{tot} , the effect of various extended mass fractions, f , was investigated (see Fig. 3).

3.1.3. BH Position as Initial Parameter

We used the position of Sgr A* as determined by Reid et al. (2003) with an uncertainty of 10 mas. When fitting non-Keplerian orbits, the location of the point mass is chosen within this error bar at 6 discrete positions - the centre value of the nominal radio position, the four extreme values determined from the error bars, and the best offset value as determined by Eisenhauer et al (2003), which is the deviation of the focus of their Keplerian orbit from the central radio position. We denote these six cases as the *center*, *northern*, *western*, *southern*, *eastern* and *offset* positions. In order to check the accuracy of the focus of the Keplerian orbit, we compare the

Table 3. Table giving the goodness of fit, χ^2_{tot} , of the best fitting orbits for the six different cases of the BH position.

BH position	$M_{tot}[M_\odot]$	$M_{cusp}[\%]$	χ^2_{tot}
Northern	3.0	10%	4.1
Western	4.0	20%	3.7
Eastern	3.3	0%	2.1
Eastern	3.65	10%	2.1
Southern	4.8	20%	1.9
Centre	3.65	5%	1.4
Offset	3.65	0%	1.09
Offset	4.1	10%	1.09
Offset	4.8	25%	1.17

two positions for the star S2 at the epoch 2002.30 calculated with the orbital parameters given by Eisenhauer et al. (2003) and by Ghez et al. (2003b). From the corresponding positions and uncertainties, an offset of the focus of the orbit of Ghez et al. (2003) from the one of Eisenhauer et al. (2003) of 0.0 ± 2.9 mas East and 0.8 ± 2.0 mas North can be derived. Hence, we find an excellent agreement between the two independent results.

3.1.4. Core radius

In order to take into account the uncertainty of the core radius of the inner cusp, the orbital fits computed for our best fitting model value of $R_1 = 15.5$ mpc, were repeated only in the case of the fitting orbits, for the extreme cases of $R_1^{min} = 13.8$ mpc and $R_1^{max} = 20.2$ mpc.

4. Results of non-Keplerian Fits

4.1. Best Fitting orbits

Our results show that the available data on the orbit of S2 can be fitted with *non-Keplerian* as well as with *Keplerian* orbits (see Fig. 4). In fact, in both cases a minimum χ^2_{tot} value of 1.1 was obtained. In other words, it cannot be excluded that apart from the black hole there exists an additional extended mass component.

In the case of Keplerian orbits and an *offset* position of the BH, the best fit is obtained for a $3.65 \times 10^6 M_\odot$ black hole. In contrast, if we assume an additional extended mass component, then the best fit is obtained for a $4.1 \times 10^6 M_\odot$ total mass with a 10% extended component, or a $4.8 \times 10^6 M_\odot$ total mass with a 25% extended component. The orbital parameters including the error bars for these three best fitting cases are given in Table. 4. Within the uncertainties the orbital parameters for the Keplerian case agree with earlier work (Schödel et al. (2003), Ghez et al. (2003), Eisenhauer et al. (2003)).

Table 4. Table of the orbital parameters of the 3 best fitting orbits in the case of the *offset* position of the BH. We also give the full parameter range [Min;Max] that produces $\chi^2_{tot} \leq 2$ orbital fits for S2. The three best fits have the smallest χ^2_{tot} and correspond to the case of the *offset* position (see Table 3). We exclude solutions with $M_{tot} > 5 \times 10^6 M_\odot$.

Total Mass M_{tot} ($10^6 M_\odot$)	3.65	4.10	4.80	Min	Max
				3.28	5.40
Point Mass M_{BH} ($10^6 M_\odot$)	3.65	3.69	3.65	3.28	3.97
Cusp Percentage(%)	0.0	10	25	0	35
e : Eccentricity	0.88	0.882	0.881	0.868	0.897
i : Inclination($^\circ$)	-47.89	-47.88	-48.12	-46.86	-50.19
a : Semi-major axis(mpc)	4.65	4.66	4.59	4.52	4.79
T : Time of peri-centre passage	2002.327	2002.328	2002.333	2002.327	2002.337
Ω : Angle of line of nodes($^\circ$)	45.3	45.38	44.59	42.17	46.1
ω : Angle to peri-centre($^\circ$)	145.1	144.84	145.6	144.1	147.7
P : Period (Years)	15.55	15.43	15.06	14.61	16.67
Peri-Centre distance	0.557	0.552	0.55	0.511	0.6
$\Delta\alpha$: Pericentre-shift per revolution	00°00'00"	00°40'48"	01°52'43"	00°00'00"	03°07'12"

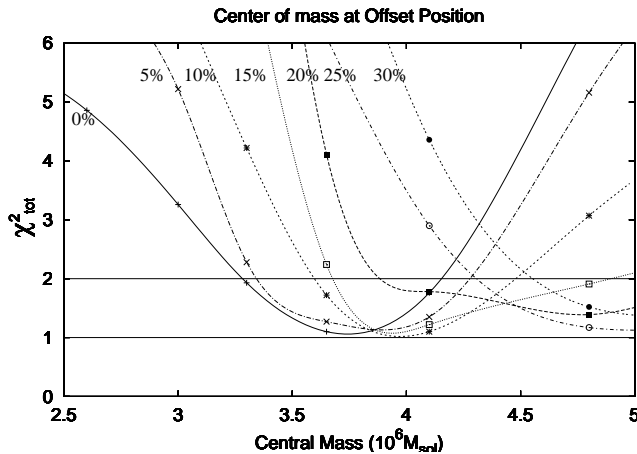


Fig. 3. Plot of the χ^2_{tot} values vs. the total central mass, M_{tot} , calculated for different extended mass fractions, f , with the point mass at the offset position. Values of the same f are fitted with splines. Crosses: $f = 0$; “x” symbols: $f = 0.05$; stars: $f = 0.1$; empty squares: $f = 0.15$; filled squares: $f = 0.2$, empty circles: $f = 0.25$; and filled circles: $f = 0.3$. For all solutions plotted here, $\chi^2_{tot} \leq 2$. The best fitting case is indicated by a star, it corresponds to the case of $M_{tot} = 4.1 \times 10^6 M_\odot$ and $f = 0.1$.

4.2. Position of Sgr A*

The three best fitting orbits were obtained for the *offset* position of the point mass, as defined in § 3. The cases of *eastern*, *northern*, *southern* and *western* position can most likely be excluded as only fits with $\chi^2_{tot} \gtrsim 2.0$ were found, meaning that in each case at least one data point had a 3σ deviation from the orbit. To give nevertheless an idea of the orbits in such cases, Fig. 5 illustrates some of them. Table 3 shows that apart from the *offset* position only the *central* position is worth considering. For the black hole at this *central* position a lowest χ^2_{tot} of 1.4 was found. In the following, we will only consider the *offset* position of the central point mass.

4.2.1. Higher total central masses and cusp masses

Fig. 4 shows a plot of χ^2_{tot} vs. different discrete central total mass values and for each fraction f of the extended mass at the offset position. We also examined orbits with total masses higher than $4.8 \times 10^6 M_\odot$, up to $8.0 \times 10^6 M_\odot$. This resulted in high masses for the inner cusp. We found that the S2 orbit could fit the data well for cusp masses up to 55%. However, the total masses in these cases are in disagreement with the dynamical mass estimates at large radii. For this reason, they are ruled out in this investigation. However, large amounts of extended mass inside the S2 orbit would be possible if the mass distribution function at the centre were steeper than in our model or if the core radius were smaller than the apo-centre of S2 (~ 9 mpc). In that case mass densities – exceeding order of magnitudes over the currently derived few $10^8 M_\odot \text{pc}^{-3}$ – are unlikely because stellar collisions will become of increasing importance.

4.2.2. Core Radius of Inner Cusp

For our best solutions (with $\chi^2_{tot} \leq 2.0$), the fitting procedure was repeated for the extreme cases of $R_1^{min} = 13.8$ mpc and $R_1^{max} = 20.2$ mpc of the inner cusp radius. Even with these different core radii, we find that the three best cases discussed above, (with (1) just a $3.65 \times 10^6 M_\odot$ black hole, (2) a $4.1 \times 10^6 M_\odot$ total mass with a 10% extended component, and (3) a $4.8 \times 10^6 M_\odot$ total mass with a 25% extended component), still give the best fits. Also the fit quality remains unchanged at $\chi^2_{tot} = 1.1$.

5. Discussion

In the previous sections it was demonstrated that the measured positions and line-of-sight velocities of S2 can be fitted by non-Keplerian orbits as well as by Keplerian orbits. Assuming a simple Keplerian case, the central gravitational potential by definition is entirely dominated by the point mass associated with Sgr A* and no dynamical constraints can be derived on

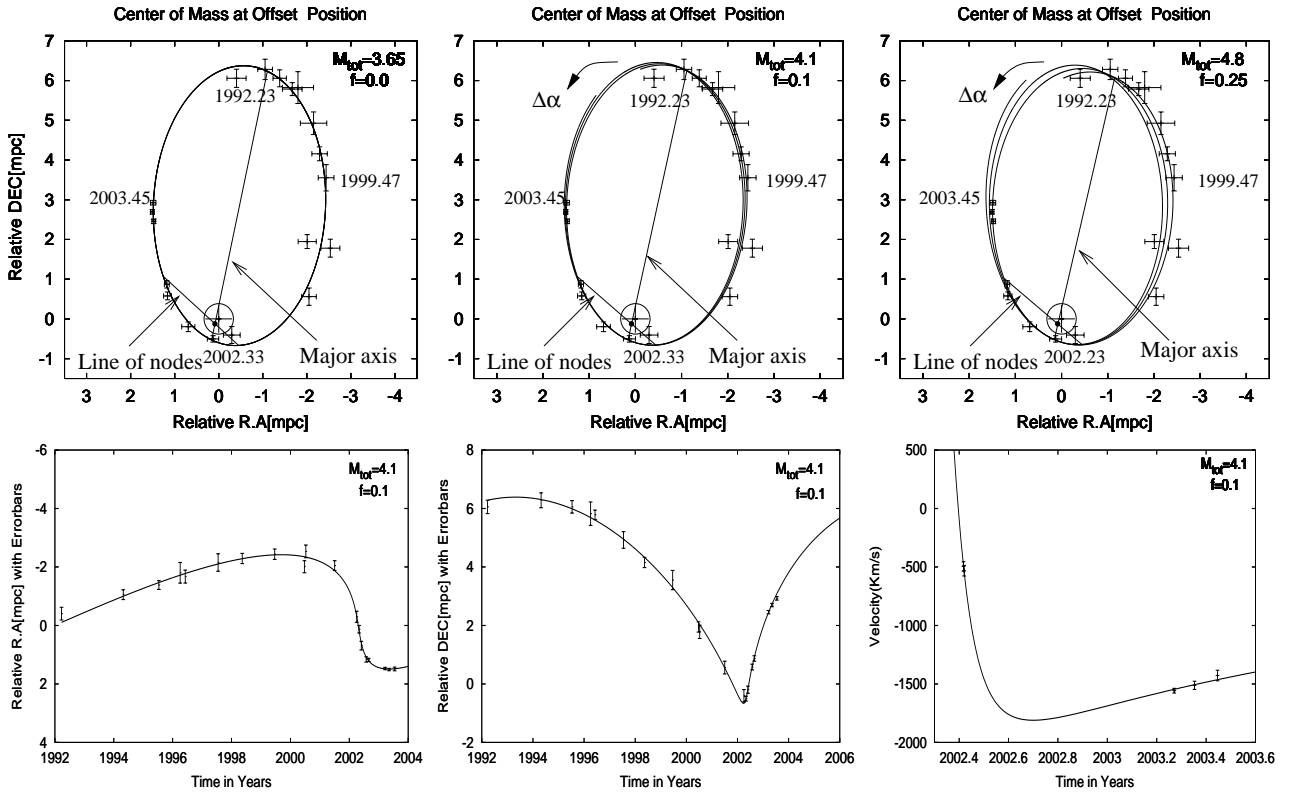


Fig. 4. Three exemplary orbits determined by our fitting. Upper left panel: Keplerian orbit with $3.65 \times 10^6 M_\odot$ point mass. Upper middle panel, non-Keplerian orbits with $4.1 \times 10^6 M_\odot$ total mass, thereof 10% extended. Upper right panel, non-Keplerian orbits with $4.8 \times 10^6 M_\odot$ total mass, thereof 25% extended. Here the central mass is at the offset position, 0.082mpc east and 0.112mpc south from the nominal radio position of Sgr A*. The lower panels show the velocity in the relative R.A., the relative Dec., and along the line-of-sight as a function of time for the case of $4.1 \times 10^6 M_\odot$ total central mass with a 10% extended component. This case is representative for the other cases. The direction of $\Delta \alpha$ the pericenter-shift is shown by an arrow.

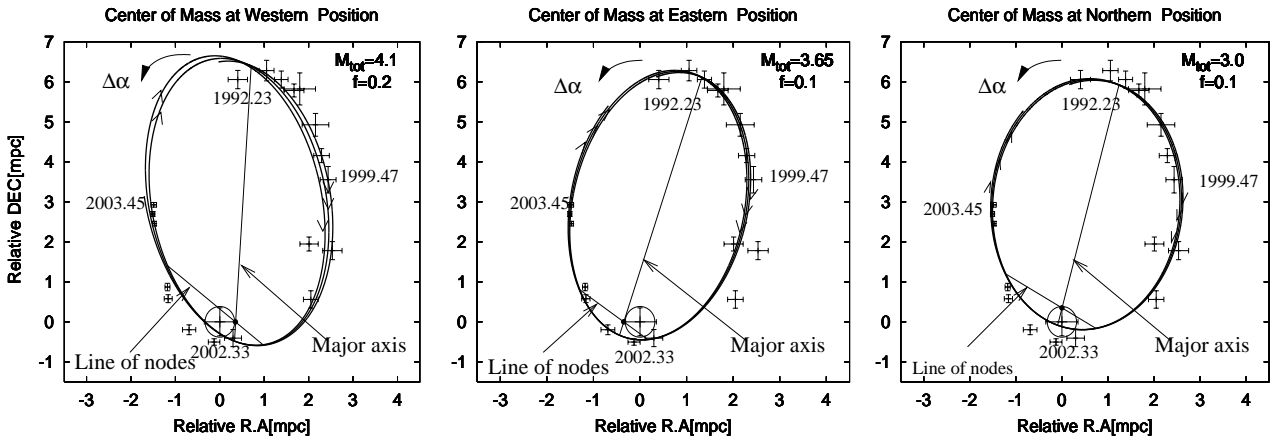


Fig. 5. Example of 3 orbits corresponding to: (Left) the case of *Western* position, a fit with $4.1 \times 10^6 M_\odot$ total mass with a 20% extended component (Middle) the case of *Eastern* position, a fit with $3.65 \times 10^6 M_\odot$ total mass with a 10% extended component, and (Right) the case of *Northern* position, a fit with $3.0 \times 10^6 M_\odot$ total mass with a 10% extended component.

any extended mass component due to e.g. the surrounding stellar cluster. More revealing, however, is the more physical assumption of non-Keplerian orbits. The presence of a stellar cusp shows that – at least to a certain extent – there is some extended mass present near the black hole. We assumed that

this potential could be modelled by the central black hole plus an extended mass component, which is distributed according to the Plummer density model of the inner cusp that was obtained by fits to stellar number density counts in § 2.

In sections §5.1 and §5.2 we focus on the question of what could be the nature of this possible extended mass component in the cusp that is higher than the $8540 M_{\odot}$ derived from stellar number density counts (section 2). The value of $8540 M_{\odot}$ representing the total mass of the 'inner cusp' is equivalent to a mass of $3100 M_{\odot}$ inside the core radius R_1 (15.5 mpc or $0.4''$). It is based on the assumption that the ratio of the stellar number counts to total stellar mass does not vary with radius and environment in the Galactic Centre (see also Genzel et al., 2003). It is very likely that this assumption is unjustified. Genzel et al. (2003) find that the stellar population in the cusp differs to a certain degree from the population of the surrounding, large-scale cluster. Also, effects such as mass segregation and stellar collisions might work very effectively in the dense environment of the cusp. Therefore, we consider that the mass-to-light ratio, M/L ($2\mu\text{m}$), of the stellar cluster varies with separation from Sgr A*. In the following, two hypotheses will be discussed: The existence of a cluster of faint low-mass stars, not yet detectable with the resolution and sensitivity of current instruments, and the existence of a cluster of heavy dark objects like stellar black holes and neutron stars.

5.1. Extending the K-band Luminosity Function to Faint Stars

We use the K -band luminosity function (KLF) for $K \leq 18$ mag within a projected radius of $1.5''$ from Sgr A* as it was determined by Genzel et al. (2003 - see their Fig.11). Note that the KLF is not corrected for extinction or for the distance modulus. The authors fitted the KLF with a power-law with a slope of $\beta = 0.21 \pm 0.03$, ($\beta = \text{dlogN/dK}$). Since this result is based on a number of roughly 60 stars within $1.5''$ of Sgr A*, the observed stars themselves cannot account for a significant extended mass component. It is therefore necessary to extrapolate the KLF at the faint end. However, we assume that the observed stars trace the mass carrying population which can currently only be accessed theoretically by extrapolating the KLF towards its faint end.

For the extrapolation of the KLF two different slopes are considered, $\beta = 0.21$ and a steeper one, $\beta = 0.35$, which fits the Bulge KLF (Alexander and Sternberg 1999) as well as a model of an old (~ 10 Gyr) stellar cluster of solar metalicity (Zoccali et al. 2003). In the following we concentrate on the region within R_1 of the inner Plummer model component. The total number of stars in the inner cusp ($R \leq 0.4''$ or 15.5 mpc) brighter than a given magnitude can be directly estimated from the (extrapolated) KLF.

The KLF gives the number of stars per surface area per magnitude. In order to calculate the total number of stars and the total stellar mass present within the spherical volume enclosed by the core radius of $R = 0.4''$ of our central Plummer model component, we de-projected the KLF. Table 6 lists the resulting numbers of stars, the total cluster mass, M_{Cl} , the average stellar mass in the cluster, M_{aver} , and the corresponding M/L ($2\mu\text{m}$) for clusters given by KLFs with slopes of $\beta = 0.21$ and $\beta = 0.35$ and for different cut-off magnitudes, between $K = 20$ ($M_{\text{min}} = 1 M_{\odot}$) and $K = 28$ ($M_{\text{min}} = 0.06 M_{\odot}$).

Table 5. Extinction free mass-to-light ratios, $M/L(2\mu\text{m})$, for different stellar types in luminosity class V at the distance of the Galactic Centre.

$M/L(2\mu\text{m})[M_{\odot}/L_{\odot}]$	K[mag]	Mass[M_{\odot}]	Spectral types
1.29	16.425	1.60	F0
1.93	17.005	1.40	F5
2.73	17.695	1.05	G0
5.02	18.665	0.79	K0
5.36	18.915	0.67	K5
11.77	20.065	0.51	M0
9.23	20.065	0.4	M2
16.66	20.915	0.33	M3
38.49	22.315	0.21	M5
87.55	23.815	0.12	M7
166.43	25.265	0.06	M8

M_{Cl} is calculated from the observed KLF using $A_K = 3$ and the M/L ($2\mu\text{m}$) values listed in Table 5.

The numbers listed in Table 6 show that the mass of stars present within $R = 0.4''$ deduced from a $\beta = 0.21$ slope KLF cannot be higher than $800 M_{\odot}$, even after extrapolation to the faintest magnitudes (see Table 5 for a list of K-magnitudes and corresponding MS-stars at the GC). Therefore, a cluster with a KLF of $\beta = 0.21$ cannot explain a mass of $3100 M_{\odot}$ within $R = 0.4''$, estimated from direct number density counts with an $M/L(2\mu\text{m}) = 2 M_{\odot}/L_{\odot}$ (see § 2).

M/L ($2\mu\text{m}$) converges to a value $2 M_{\odot}/L_{\odot}$ for $\beta = 0.35$, and a magnitude limit between 26 and 27, in this case we find the value of $3100 M_{\odot}$ required by our mass distribution modelling in § 2. Lower magnitude limits would increase M/L ($2\mu\text{m}$) further, and the mass of the inner cusp calculated from our Plummer model would be underestimated. Stellar types corresponding to the required M/L ($2\mu\text{m}$) ratios are listed in Table 5.

Table 6 also shows that for a main-sequence stellar population $M/L(2\mu\text{m})$ does not exceed $4.0 M_{\odot}/L_{\odot}$, even if we consider very faint/low-mass stars ($K = 28$) and a steep faint-end KLF ($\beta = 0.35$). This is much smaller than the value of $96 M_{\odot}/L_{\odot}$ possible within our best fitting case of 10% cusp and a total mass of $4.1 \times 10^6 M_{\odot}$. We conclude that the best fitting case of a non-Keplerian orbit for S2 allows for an extended mass component that is far too large to be explained by a stellar population of MS stars, and therefore would require another type of mass carriers. We show in § 5.3 that such a configuration is possible.

5.2. Stability of a Cluster of Low-Mass Stars

For a multi-mass stellar distribution, high mass stellar remnants (stellar black holes and/or neutron stars) are expected to migrate to the centre as a consequence of dynamical friction. One would expect that, within a Hubble time, these compact objects show a higher concentration toward the centre than the lighter ones (Morris et al., 1993; Escudé & Gould, 2000), which should be transferred by that mechanisms to orbits at greater distances from the centre of the cluster. This argues against the existence of a cluster of low-mass stars in the inner cusp.

Table 6. For each 'observed' K-magnitude limit (not corrected for extinction) we give the numbers of stars N , cluster mass M_{Cl} , average stellar masses M_{aver} , and mass-to-luminosity ratio, $M/L(2\mu\text{m})$, within the central $0.4''$ for hypothetical Plummer model type clusters with KLFs extrapolated by two power-law slopes of $\beta = 0.21$ and $\beta = 0.35$. M_{Cl} is the mass inside the core radius R_1 of the innermost Plummer model component. The derived M/L values include an extinction correction for $A_K=3$.

Magnitude limit	$\beta=0.21$				$\beta=0.35$			
	N	$M_{Cl}[\text{M}_\odot]$	$M_{aver}[\text{M}_\odot]$	$M/L(2\mu\text{m})[\text{M}_\odot/\text{L}_\odot]$	N	$M_{Cl}[\text{M}_\odot]$	$M_{aver}[\text{M}_\odot]$	$M/L(2\mu\text{m})[\text{M}_\odot/\text{L}_\odot]$
$K \leq 28$	3500	800	0.9	1.0	44500	5200	0.1	3.7
$K \leq 27$	2200	710	1.4	0.9	20000	3700	0.15	2.8
$K \leq 26$	1350	620	2.3	0.8	9000	2400	0.3	1.8
$K \leq 25$	820	525	3.7	0.7	4100	1500	0.8	1.1
$K \leq 24$	510	450	6.0	0.6	1920	1000	1.6	0.8
$K \leq 23$	310	390	10	0.5	950	700	3.3	0.5
$K \leq 22$	190	325	16	0.4	510	480	6.0	0.4
$K \leq 21$	120	235	26	0.4	320	380	9.7	0.3
$K \leq 20$	70	193	42	0.3	230	270	11.2	0.2

Table 7. Mass-to-light ratios $M/L(2\mu\text{m})$, for the different offset position fitting orbits obtained from our model calculations. The errors on M/L are model dependent. From scaling to the enclosed mass estimate in Fig. 2 we estimate an error of 5%.

M_{tot}	f	$M/L(2\mu\text{m})[\text{M}_\odot/\text{L}_\odot]$
3.65	0.0	2.00
3.65	0.05	42.74
3.65	0.10	85.48
4.10	0.05	48.01
4.10	0.10	96.02
4.10	0.15	144.03
4.10	0.20	192.04
4.80	0.20	224.82
4.80	0.25	269.32
4.80	0.30	337.24

On the other hand, the possibility of a cluster of low-mass stars cannot be excluded and we are far from understanding the properties of the stars in the cusp. There is for example the unexplained presence of massive young stars, e.g. MS O/B-type stars close to the black hole (Genzel et al., 1997; Eckart, Ott & Genzel, 1999; Figer et al., 2000; Gezari et al., 2002; Ghez et al., 2003). These stars have not had enough time to achieve energy equipartition with the fainter older stellar population. They are hence dynamically un-relaxed. Also, there are indications for a radial anisotropy of the stars in the cusp which might be un-relaxed (Schödel et al., 2003), in spite of the expected short relaxation time in this dense environment. Because of this general lack of theoretical understanding of the cluster near Sgr A*, we consider that a cluster of faint/low mass stars should not be ruled out entirely from the possible interpretations of the inner cusp.

5.3. Is the Cusp Dominated by Dark and Massive Objects?

A result of our model calculations is that a possible best solution for the orbital fits of star S2 can be achieved with a black hole mass of $M_{BH}=3.65\times 10^6\text{M}_\odot$ and a cusp mass of 10% or less i.e. $M_{cusp}\leq 1.5\times 10^5\text{M}_\odot$. The evaluation presented in § 5.1

shows that such a heavy cusp is unlikely to consist of stars only. The combination of stellar evolution (production of stellar mass black holes, neutron stars, white dwarfs, and of binaries including such objects) and stellar dynamics will almost certainly lead to a strong increase of M/L in the central parts of the nuclear star cluster. Black holes and neutron stars sink to the centre and may coalesce (Gürkan et al. 2003). If there is an aged stellar population like in globular clusters strong M/L variations may even be created by segregation of white dwarfs to the center, since they are on average more massive than low-mass main sequence stars (Baumgardt et al. 2003). Such detailed modeling of a cluster with already a pre-existing supermassive black hole in a dense stellar cluster, as in the centre of our Galaxy, is not yet available. It is, however, a fair conclusion that strong dynamically caused M/L variations prevail also in such case, see for an approximate model of such situation also Murphy, Cohn & Durisen (1991). In the following we investigate if high M/L stellar remnants can form a stable configuration.

Rauch & Tremaine (1996) studied the configuration of a central massive black hole plus an extended mass distribution M of radius R consisting of objects with mass m in terms of its non – resonant relaxation time t_{rel}^{nr} . Under the assumption that $M \ll M_{BH}$, Rauch & Tremaine (1996) derive how t_{rel}^{nr} depends on M_{BH} , M , and the orbital time scale t_{orb} at the outer edge of the cluster. If (a) the stellar orbits have random orientations and moderate eccentricities, (b) the density of stars is approximately uniform within R , and (c) $M_{cluster} / M_{BH} = 10^{-2} - 10^{-5}$ then Rauch & Tremaine (1996) find that

$$t_{rel}^{nr} \sim \frac{M_{BH}^2}{m^2 N \ln \Lambda} t_{orb}, \quad (6)$$

where $\ln \Lambda$ is the Coulomb logarithm ~ 13 in this case. This situation should - to first order - be applicable to the Black Hole/cusp scenario at the Galactic centre. Condition (a) is probably fulfilled with the possible exception that the stars in the cusp might have fairly high eccentricities (Schödel et al. 2003). Assuming a Plummer model as a cusp description fulfills condition (b). For our best fits with cusp masses of $\leq 10\%$ we find that M/M_{BH} is of the order of 10^{-2} , if we restrict ourselves to

the region within the core radius R_1 . This is close to what is required by condition (c).

Here, $M_{BH} = 3.65 \times 10^6$ and m_{sr} is the average mass of the stellar remnants. A value of $m_{sr} = 5 M_\odot$ is roughly consistent with a composite cluster made of neutron stars ($m \sim 1.5 M_\odot$) and stellar black holes ($5 M_\odot < m < 25 M_\odot$). We then find that $t_{rel}^{nr} \sim 10^6 \times t_{orb}$, if we assume that most of the mass inside the core radius is present in the form of stellar remnants of average mass m_{sr} . Considering that the core radius of 15-20 mpc will define t_{orb} we find t_{rel}^{nr} to be about 2×10^7 years.

We can also investigate whether such a configuration is stable by estimating how many stellar black holes evaporate. Integrating a Maxwell distribution function for the velocities above the escape velocities gives the percentage of stars not bound to the BH. For the velocity dispersion, following Alexander et al. (2003), we can write:

$$v_{\text{escape}} = \sqrt{2} v_{\text{circular}} = \sqrt{2(1+\alpha)} \sigma. \quad (7)$$

For a value of $\alpha = 2$, about 0.03% of the present stellar black holes will be evaporated after each relaxation time. For a steeper cusp with $\alpha=3$ we find that 0.006% of the stellar black holes will evaporate on that time scale. For t_{rel}^{nr} of a few 10^7 years and α between 2 and 3 about 50% of the stellar black holes will have evaporated after 25 to 250 t_{rel}^{nr} corresponding to about 5×10^8 to 5×10^9 years. Given the fact that there will also be an influx of mass i.e. stellar black holes or neutron stars from outside the cusp one can consider such a configuration stable over a significant fraction of the Milky Way's age.

6. Summary

From stellar number counts, we have strong reason to assume that there is some extended mass around Sgr A*. Therefore, orbits of stars near Sgr A* should be analysed in terms of non-Keplerian motion. Only in that way it is possible to find out more about the composition of the cusp. This paper presents the first approach to this problem. In this work we studied the case where the contribution of the central stellar cluster at the centre of the Milky Way could introduce pericentre-shifts of the order of 1 degree per revolution on the orbit of S2. We assume that the dynamics of S2 is governed by both the super-massive black hole and the central cluster. The steeply rising, cusp-like stellar density distribution in the inner few tens of milli-parsecs near Sgr A* can be modelled with a Plummer model distribution having a relatively small core radius of the order of the S2 semi-major axis. In a spherical potential, the stellar orbits will precess and the stars will follow rosetta shaped trajectories (Binney & Tremaine, 1987; Rubilar & Eckart, 2001; Fragile, & Mathews, 2000). We performed orbital fits to the S2 data for this class of orbits. We used a fourth order Hermite integrator, adequate for the required precision. The runs were performed for a large range of initial parameters for the total mass, the position of the centre of mass, the fraction of the extended mass component, and the 6 classical orbital parameters.

We found that the S2 trajectory can be equally well fitted by *non-Keplerian* orbits as by *Keplerian* orbits. For the Keplerian case, we could confirm the results of Schödel

et al. (2003), Ghez et al. (2003), and Eisenhauer et al. (2003). Basically independent of the amount of total or extended mass we find consistently a value for the central Black Hole mass of about $3.7 \times 10^6 M_\odot$. This is well between but not coincident with one of the two possible Black Hole mass estimates of either $4.75 \times 10^6 M_\odot$ or $2.79 \times 10^6 M_\odot$ that were derived by Aschenbach et al. (2003) from an analysis of the quasi-periodicity observed in strong X-ray flares.

Our best solution in the case of *non-Keplerian* orbits implies a total mass of $4.1 \times 10^6 M_\odot$ with the fraction of the extended mass being $f = 0.1$. With this value of f , the amount of mass present in the inner cusp is 50 times larger than the one expected from a direct mass estimation deduced from the stellar density and the integrated mass plot (see Fig. 1 and Fig. 2) and assuming a constant $2\mu\text{m}$ mass-to-light ratio of $2 M_\odot/L_\odot$.

If the inner cusp is mainly composed of main sequence stars, then a $M/L(2\mu\text{m})$ of $2 M_\odot/L_\odot$ can only be attained in the case of a faint-end KLF slope of $\beta = 0.35$ and a magnitude limit $25 < K < 26$. The mass of such a cluster will be $3100 M_\odot$ within $R = 15$ mpc derived from our initial Plummer model in § 2. The existence of even fainter ($K < 28$), low-mass stars ($0.06 M_\odot$) in the inner cusp will not contribute more than ~ 3 times the mass in the inner cusp; such a configuration is not likely to be stable for a long time. In addition it would be unclear how these stars would get into the inner cusp. It is unlikely that they formed there, however, they might have migrated into that region by loosing angular momentum by interactions with stars in the overall Galactic Centre stellar cluster with a core radius of 0.3-0.4pc.

Our best solution with a total mass of $4.1 \times 10^6 M_\odot$ and an extended mass component of 10% implies an $M/L(2\mu\text{m})$ of $\sim 96 \pm 10 M_\odot/L_\odot$; here objects with large M/L values are needed to explain the extended cusp mass. One plausible explanation could be the presence of a cluster of massive stellar remnants. By applying (eq. 6) we find that an equilibrium configuration is possible under certain conditions.

In this study relativistic effects were not included for the orbit of the star S2. The peri-centre shift induced by relativistic effects is of the order of 9 arcmin compared to the 40 arcmin expected from the Newtonian shift due to the presence of an extended mass (see also Rubilar & Eckart, 2001, Fragile, & Mathews, 2000). It should be pointed out that the peri-centre shift due to relativistic effects is in the opposite direction of that due to the extended mass and that relativistic effects could in a way mask the amount of extended mass around the black hole. Therefore it will be important for future work to investigate relativistic effects in more detail.

After only a few additional observational epochs it will be possible to put even stronger constraints on the mass of the cusp, and consequently to know more about the mass carrying population in the immediate vicinity of the black hole at the centre of the Milky Way.

As discussed in Rubilar & Eckart (2001) a complete determination of the cusp parameters can be expected from combinations of 3 or more orbits since then the number of degrees of freedom for the fits is increasing rapidly. Further studies with more general density distributions should be undertaken,

because they may influence the precise value of the extended mass contribution.

Acknowledgements. N. Mouawad thanks M. Freitag for substantial discussions. This work has been partly supported by the Deutsche Forschungsgemeinschaft (DFG) via grant SFB439 at the University of Heidelberg and SFB494 at the University of Cologne.

References

Aarseth, S.J. 1999, Pub. Astron. Soc. Pac , 111, 1333

Alexander,T. 1999, ApJ, 527,Issue 2,835

Alexander, Tal & Sternberg, Amiel, 1999, ApJ, 520, 137A

Alexander,T. 2003, In: The Galactic black hole. Lectures on general relativity and astrophysics. Edited by Heino Falcke; Friedrich W. Hehl. Series in high energy physics, cosmology and gravitation. Bristol: IoP, Institute of Physics Publishing, ISBN 0-7503-0837-0, 2003, p. 246-274

Aschenbach, B., Grosso, N., Porquet, D., Predehl, P., A&A accepted, astro-ph/0401589

Baganoff, F.K., et al. 2001, Nature, 413, 45

Baumgardt, H., Hut, P., Makino, J., McMillan, S., & Portegies Zwart, S. 2003, ApJ, 582, L21

Binney, J. & Tremaine, S. 1987, Galactic Dynamics, Princeton Series in Astrophysics

Eckart, A., Genzel, R., Hofmann, R., Sams, B. J.& Tacconi-Garman 1995, ApJ, 445, L23

Eckart, A. & Genzel, R. 1996, Nature, 383, 415

Eckart, A., Genzel, R., Ott, T. & Schödel, R. 2002a, MNRAS, 331, 917

Eckart, A., Mouawad, N., Krips, M., Straubmeier, C., and Bertram, T., 2002, SPIE 4835-03, Cnf. Proc. of the SPIE Meeting on 'Astronomical Telescopes and Instrumentation', held in Waikoloa, Hawaii, 22-28 August 2002b

Eckart, A., Bertram, T., Mouawad, N., Viehman, T.,Straubmeier, C., Zuther, J. 2002, Contribution to the JENAM meeting on: The VLTI - Challenges for the Future, Porto, Portugal, September 4-7, 2002c

Eisenhauer, F., Schdel, R., Genzel, R., Ott, T., Tecza, M., Abuter, R., Eckart, A. & Alexander, T. 2003, ApJ, 597, Issue 2, L121

Ferrarese, L., Pogge, R. W., Peterson, B. M., Merritt, D., Wandel, A., & Joseph, C. L. 2001, ApJ, 555, L79

Figer, Donald F., Becklin, E. E., McLean, Ian S., Gilbert, Andrea M., Graham, James R., Larkin, James E., Levenson, N. A., Teplitz, Harry I., Wilcox, Mavourneen K., Morris, Mark, 2000, ApJ, 533L, 49F

Fragile, P.C. & Mathews, J., 2000, ApJ 542, 328

Genzel, R., Hollenbach, D. J., Townes, C. H., Eckart, A., Krabbe, A., Lutz, D. & Najarro, F.t., 1994, NATO Advanced Science Institutes (ASI), Series C, 445, 327

Genzel, R., Eckart, A., Ott, T., & Eisenhauer, F., 1997, MNRAS, 291, 219G

Genzel, R., Pichon, C., Eckart, A., Gerhard, O. & Ott, T., 2000, MNRAS, 317, 348

Genzel, R., Schdel, R., Ott, T., Eisenhauer, F., Hofmann, R., Lehnert, M., Eckart, A., Alexander, T., Sternberg, A., Lenzen, R., Cnet, Y., Lacombe, F., Rouan, D., Renzini, A. & Tacconi-Garman, L. E. 2003, ApJ, 594, Issue 2, 812

Gezari, S., Ghez, A. M., Becklin, E. E., Larkin, J., McLean, I. S., Morris, M., 2002, ApJ, 576, 790G

Ghez, A. M., Klein, B. L., Morris, M. & Becklin, E. E. 1998, ApJ, 509, Issue 2, 678

Ghez, A., Morris, M., Becklin, E.E., Tanner, A. & Kremenek, T. 2000, Nature, 407, 349

Ghez, A., Duchêne, G., Matthews, K., Hornstein, S. D., Tanner, A., Larkin, J., Morris, M., Becklin, E. E., Salim, S., Kremenek, T., Thompson, D., Soifer, B. T., Neugebauer, G., & McLean, I. 2003a, ApJ, 586, L127

Ghez, A., Salim, S., Hornstein, S. D., Tanner, A., Morris, M., Hecklin, E. E. & Duchêne, G. 2003b, astro-ph/0306130

Gürkan et al. 2003, astro-ph/0308449

Kormendy, J. & Richstone, D. 1995, Annu. Rev. Astron. Astrophys., 33, 581

Kormendy, J. 2001, Rev. Mexicana Astron. Astrofis. Ser. Conf., 10, 69

Lo, K. Y., 1985, Proceedings of the ESO-IRAM-Onsala Workshop on (Sub)Millimeter Astronomy, Aspasia, Sweden, June 17-20, 1985, 273 sma..work..273L

Makino, J. & Aarseth, S.J. 1992, Proc. Astron. Soc. Japan, 44, 141

Maoz, E. 1998, ApJ, 494, 181

Melia, F. & Falcke, H. 2001, Annu. Rev. Astron. Astrophys. 2001, 39, 309

Mezger, P. G., Duschl, W. J. & Zylka, R. 1996, Astron. Astrophys. Rev., 7, 289

Morris, M. 1993, ApJ, 408, 496

Morris, M. & Serabyn, E. 1996, Annu. Rev. Astron. Astrophys. 1996, 34, 645

Munyaneza, F. & Viollie, R. D. 2002, ApJ, 564, 274

Murphy, B.W., Cohn, H.N., Durisen, R.H., 1991, ApJ 370, 60

Ott, T., Eckart, A. & Genzel, R. 2000, ApJ, 523, 2480

Ott, T. 2003, PHD Thesis, Ludwig-Maximilians-Universität, München

Rauch, Kevin P. & Tremaine, Scott, 1996, 1996, New A, 1, 149R

Reid, M. J., Menten, K. M., Genzel, R., Ott, T., Schdel, R. & Eckart, A., 2003, ApJ, 587, 208

Reid, M. J. 1993, Annu. Rev. Astron. Astrophys., 31, 345

Rubilar, G. F.& Eckart 2001, A., A&A, 374, 95

Spitzer, L. Jr. 1975, Dynamical Evolution of Globular Clusters, Princeton Series in Astrophysics

Spurzem, R. 1999, J. Comp. Appl. Math, 109, 407

Schödel, R., Ott, T., Genzel, R., Hofmann, R., Lehnert, M., Eckart, A., Mouawad, N., Alexander, T., Reid, M. J., Lenzen, R., Hartung, M., Lacombe, F., Rouan, D., Gendron, E., Rousset, G., Lagrange, A.-M., Brandner, W., Ageorges, N., Lidman, C., Moorwood, A. F. M., Spyromilio, J., Hubin, N., Menten, K. M. 2002, Nature, 419, 694

Schödel, R., Ott, T., Genzel, R., Eckart, A., Mouawad, N., Alexander, T. 2003, ApJ, 596, 1015

Schödel, R., 2004, PHD Thesis, Ludwig-Maximilians-Universität, München

Zoccali, M., Renzini, A., Ortolani, S., Greggio, L., Saviane, I., Cassisi, S., Rejkuba, M., Barbuy, B., Rich, R. M., Bica, E., 2003, A&A, 399, 931Z